Original article

Nuclear Medicine Communications

Combined fuzzy logic and random walker algorithm for PET image tumor delineation

Motahare Soufi[a], Alireza Kamali-Asl[a], Parham Geramifar[b], Mehrsima Abdoli[c] and Arman Rahmim[d,e]

Purpose **The random walk (RW) technique serves as a powerful tool for PET tumor delineation, which typically involves significant noise and/or blurring. One challenging step is hard decision-making in pixel labeling. Fuzzy logic techniques have achieved increasing application in edge detection. We aimed to combine the advantages of fuzzy edge detection with the RW technique to improve PET tumor delineation.**

Methods **A fuzzy inference system was designed for tumor edge detection from RW probabilities. Three clinical PET/computed tomography datasets containing 12 liver, 13 lung, and 18 abdomen tumors were analyzed, with manual expert tumor contouring as ground truth. The standard RW and proposed combined method were compared quantitatively using the dice similarity coefficient, the Hausdorff distance, and the mean standard uptake value.**

Results **The dice similarity coefficient of the proposed method versus standard RW showed significant mean improvements of 21.0 ± 7.2, 12.3 ± 5.8, and 18.4% ± 6.1% for liver, lung, and abdominal tumors, respectively, whereas the mean improvements in the Hausdorff distance were 3.6 ± 1.4, 1.3 ± 0.4, 1.8 ± 0.8 mm, and the mean improvements in SUVmean error were 15.5 ± 6.3, 11.7 ± 8.6, and 14.1 ± 6.8% (all *P*'s < 0.001). For all tumor sizes, the proposed method outperformed the RW algorithm. Furthermore, tumor edge analysis demonstrated further enhancement of the performance of the algorithm, relative to the RW method, with decreasing edge gradients.**

Conclusion **The proposed technique improves PET lesion delineation at different tumor sites. It depicts greater effectiveness in tumors with smaller size and/or low edge gradients, wherein most PET segmentation algorithms encounter serious challenges. Favorable execution time and accurate performance of the algorithm make it a great tool for clinical applications.** *Nucl Med Commun* **37:171–181**
Copyright © 2016 Wolters Kluwer Health, Inc. All rights reserved.

Nuclear Medicine Communications 2016, **37**:171–181

Keywords: fuzzy logic, PET, random walk, segmentation

[a]Department of Radiation Medicine Engineering, Shahid Beheshti University, [b]Research Center for Nuclear Medicine, Shariati Hospital, Tehran University of Medical Sciences, Tehran, Iran, [c]Department of Radiation Oncology, the Netherlands Cancer Institute, Amsterdam, The Netherlands, Departments of [d]Radiology and [e]Electrical & Computer Engineering, Johns Hopkins University, Baltimore, Maryland, USA

Correspondence to Alireza Kamali-Asl, PhD, Department of Radiation Medicine Engineering, Shahid Beheshti University, GC, Tehran 1983969411, Iran
Tel: +98 21 2990 4227; fax: +98 21 2243 1780; e-mail: a_kamali@sbu.ac.ir

Received 6 August 2015 **Revised** 5 October 2015 **Accepted** 5 October 2015

Introduction

PET is an increasingly prevalent modality as utilized in oncologic applications [1]. Accurate tumor volume delineation in PET images plays an essential role in treatment planning (target volume definition) as well as therapy response evaluations [2,3]. Furthermore, PET-based volumetric markers that assess disease burden and tumor aggressiveness, such as metabolic tumor volume and total lesion glycolysis, have been increasingly shown to outperform conventional SUV-based markers in prognostication of certain cancer types [4–14]. In any case, because PET images are impacted by statistical noise as well as limited spatial resolution, the latter manifesting itself in the partial volume effect (PVE) [15–18], the accuracy and reproducibility of tumor delineation can be significantly degraded, especially in tumors with complex shapes and/or heterogeneous uptake [19].

Methods based on thresholding are the most common approach for tumor segmentation applications [20–25]. Some of them may use fixed thresholds, based on values derived from phantom studies (e.g. SUV = 2.5 or 30–75% of the maximum activity of a predefined region), to delineate lesions from the background in a given region of interest drawn manually. In these approaches, the optimal threshold depends on the tumor-to-background ratios. However, adaptive thresholding techniques dynamically adapt the threshold on the basis of a desired metric such as the tumor-to-background ratio, the mean background intensity, and the estimated mean target intensity [26]. Adaptive thresholding techniques, however, need to be calibrated and optimized for each PET

Data were presented previously at the annual meeting of the AAPM, Anaheim, July 2015, and were published as a conference proceedings abstract: SU-D-201-06 – Random walk algorithm seed localization parameters in lung positron emission tomography (PET) images.

0143-3636 Copyright © 2016 Wolters Kluwer Health, Inc. All rights reserved.

DOI: 10.1097/MNM.0000000000000428

Copyright © 2016 Wolters Kluwer Health, Inc. All rights reserved.

scanner and its specific acquisition and processing protocol [27]. Furthermore, the segmentation results are sensitive to PVE and motion artifacts.

Because of the limitations of manual and thresholding techniques, researchers have proposed different semi-automatic and automatic techniques to address the challenges with PET image segmentation [28]. The random walker algorithm [29] is a graph-based image segmentation method proposed to eliminate the small-cut problem in graph cut approaches. Graph cut approaches are initialized with user-defined foreground and background seeds, and subsequently, the algorithm attempts to find a cut between object and background seeds, which has minimum sum of edge weights, to segment the object region from background. These approaches are noise sensitive, and a common problem with these methods is the 'small-cut' behavior. As the technique attempts to minimize the total edge weights in the cut, it may return a cut that merely separates the foreground from background seeds and generates smaller-than-true segments. Therefore, additional user interaction would be necessary to address this problem. The RW method has been shown to depict robustness to noise and acceptable performance in the presence of weak boundaries, motivating increased application of this technique for PET image target definition purposes [30–36]. Specifically, the random walker algorithm enables strong tumor delineation results in clinical data [34,36], and the superiority of the algorithm in contrast to other state-of-the-art techniques has been illustrated in PET image tumor segmentation [34]. Nonetheless, despite its considerable capabilities, this method has difficulty in determining object details. Decision-making with regard to an unknown pixel is a hard decision process with binary values (0 or 1) from calculated probabilities. Fuzzy logic enables production of results with assigned degrees of truthfulness and falsehood [37]. This feature has made the fuzzy logic technique a beneficial tool in many real-world applications including medical image segmentation [38–45].

The aim of the present study was to combine the benefits of fuzzy logic and the random walker algorithm. We utilized a fuzzy logic edge-detection algorithm for decision-making given random walker algorithm probabilities to enhance performance accuracy in tumor edge delineation.

Materials and methods

Random walker algorithm

The random walker algorithm is a graph-based image-segmentation technique that treats the image as a graph, in which the image pixels form the graph nodes and the graph edges are weighted using pixel intensity differences through a classical Gaussian weighting function specified with the following equation [29]:

$$w_{ij} = \exp\left(-\beta\left(I_i - I_j\right)^2\right), \tag{1}$$

where β is the free parameter and I is the image intensity at pixel i.

To enhance segmentation reproducibility, an automatic seed localization process is considered [36]. A median filter is first utilized, and then, the uptake regions of interest are determined using a thresholding function:

$$c(I) = \left\{ \begin{array}{ll} 1, & I \in \left[\frac{\mathrm{SUV}_{\max}^{\mathrm{global}}}{N}, \mathrm{SUV}_{\max}^{\mathrm{global}}\right] \\ 0, & \text{otherwise} \end{array} \right\}, \tag{2}$$

where I and $\mathrm{SUV}_{\max}^{\mathrm{global}}$ denote the pixel intensity and the maximum SUV in the slice of interest, respectively, and N is set to 2 in the present work (suggested range is $N \geq 1.5$, according to Bagci *et al.* [34]).

Fig. 1

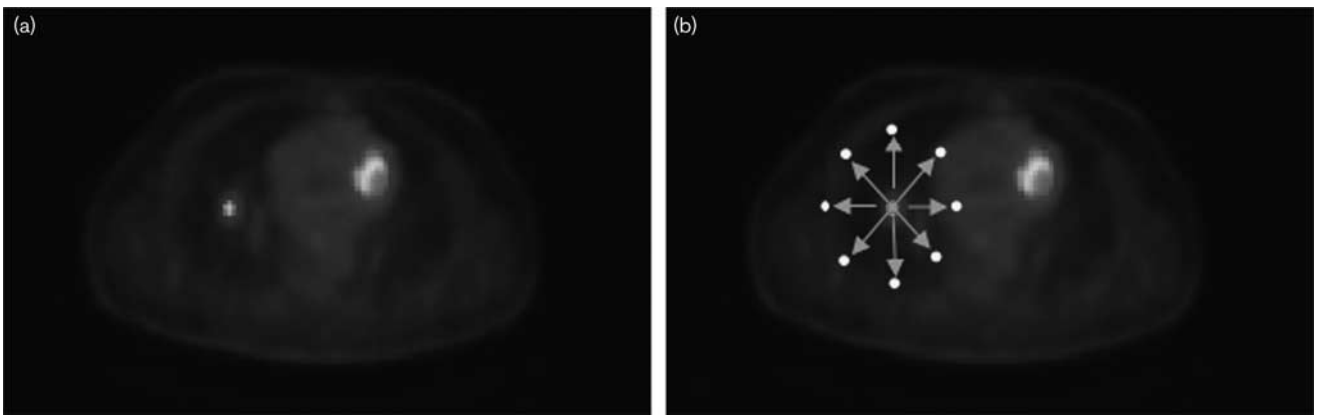

(a) A PET image of a tumor in the lung. (b) A schematic of the background seed (marked in white) localization process in eight directions has been illustrated for one foreground seed.

Copyright © 2016 Wolters Kluwer Health, Inc. All rights reserved.

On the basis of a previous study by our group [31], for each determined uptake region, pixels with greater than 70% maximum region activity were considered as foreground seeds. For each foreground seed, the neighboring pixels were searched in eight directions to find the location of the nearest pixel with value less than 30% of the maximum region activity, subsequently labeled as background. Figure 1 shows a scheme for the background seed localization for a given foreground seed point in a lung tumor. RW probabilities are then calculated for the uncertain voxels (i.e. not foreground or background) by solving a system of linear equations that compute which region a random walker from the unclassified voxels is likely to reach first (the fundamental idea behind the random walker algorithm). The final segmentation is obtained by labeling a pixel as seed pixel for which it has the highest probability of reaching [29].

Fig. 2

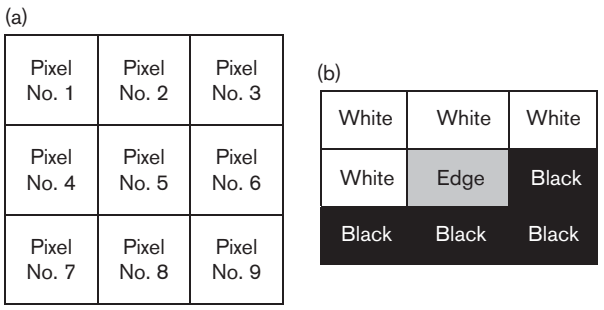

(a) Scanning mask for inputs and output determination. (b) Example of labeling the output pixel on the basis of the neighbor pixels.

Proposed method

As mentioned above, the aim of the study was to improve the performance accuracy of the random walker segmentation method using a fuzzy logic edge-detection algorithm. Unlike conventional logic, which provides hard binary outputs (i.e. 0 or 1, true or false), fuzzy logic generates a degree of truthfulness and falsehood as an output [46]. A fuzzy inference system (FIS) includes a set of rules, which are mathematical tools that simulate natural language queries to calculate values between absolute truth and absolute false [37].

In the proposed method, a set of fuzzy edge-detection rules were utilized for boundary approximation to assist in decision-making with regard to object edges. Similar to the random walker algorithm, following generation of edge weights and defining foreground and background seeds, unseeded pixel probabilities were calculated. In the last step, instead of hard decision-making with regard to the probabilities for unlabeled pixels, a set of fuzzy rules were defined and implemented for object boundary determination. As such, an FIS with image edge-detection capability was developed. The algorithm has eight inputs (pixels surrounding the central voxel) and returns one output. The system inputs are the random walker pixel probabilities, as determined from a 3×3 floating matrix mask that scans the image (Fig. 2a).

The membership functions considered for inputs and output were trapezoidal and triangular functions, respectively. Two fuzzy sets, namely black (B) and white (W) were designed for input variables, whereas three fuzzy sets including B, W, and edge (E) were used for the output. Schemes of the input and output fuzzy set membership functions are shown in Fig. 3a and b, respectively.

The first step in the fuzzy inference process is fuzzification of input variables. The FIS input is a crisp numerical value that is set as the random walker probability. The fuzzification process takes inputs and specifies their degree of belonging to each input fuzzy set (B and W) through trapezoidal membership functions (as shown in Fig. 3). Our FIS was built on 28 rules. Before evaluation of rules, all inputs must be fuzzified according to each antecedent or premise (if-part of the rule). Some of the used rules in the proposed FIS are as follows:

(1) If all eight inputs are W, then the output is W.
(2) If all eight inputs are B, then the output is B.
(3) If input pixels No.1 through No.4 are W and input pixels No.6 through No.9 are B, then the output is edge (Fig. 2b).

To obtain one number representing the result of each rule, a fuzzy 'and' operator based on the minimum method is applied. The final implication process for each rule was performed using the 'and' operator (minimum), which truncates the output fuzzy membership function by the obtained number from the fuzzy 'and' operator step. As the final decision for each set of inputs was based on checking all the rules, the truncated membership functions from all rules were combined through the maximum operation aggregation method. To obtain a single output from the resulting fuzzy set, defuzzification was performed using the centroid defuzzification technique, which returns the center of the area under the output fuzzy set function. The interested reader can refer to references [39,42,44].

Clinical study

The proposed method was applied to clinical PET images to evaluate its performance in clinical applications. Patients with solid liver, lung, and abdominal tumors were included.

The clinical datasets include PET/computed tomography (CT) scans of 12 liver, 13 lung, and 18 abdominal cancer patients, acquired on the Siemens Biograph PET/CT scanner (Siemens, Erlangen, Germany). The protocol involved ^{18}F-fluorodeoxyglucose-PET whole-body

Copyright © 2016 Wolters Kluwer Health, Inc. All rights reserved.

Fig. 3

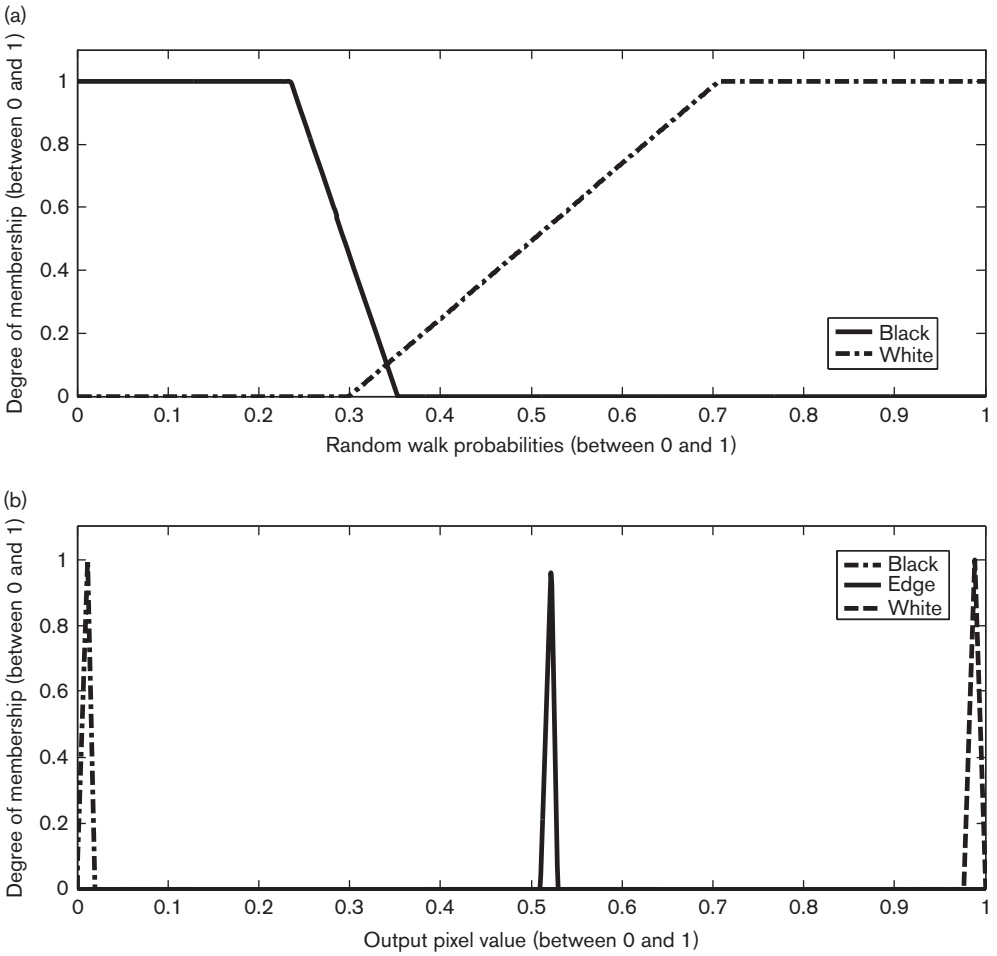

(a) FIS trapezoidal membership functions for inputs, and (b) FIS triangular membership functions for output. FIS, fuzzy inference system

imaging with low-dose CT acquisition, with an acquisition time of 3 min/bed position. Images were reconstructed using iterative TrueX (two iterations, 21 subsets), with scatter and CT-based attenuation correction. The reconstructed PET images had a matrix size of $168 \times 168 \times 252$, with voxel dimensions $4 \times 4 \times 5\ \mathrm{mm}^3$.

Manual contouring was a consensus contouring performed by two nuclear medicine experts (a single final delineation), with the results being considered as the ground truth. Quantitative performance analysis was carried out by comparing the segmentations for the random walker as well as proposed techniques against manual contouring as ground truth.

Quantitative analysis

The Dice similarity coefficient (DSC) [47] was used to quantify the performance accuracy of the random walker and proposed methods. Spatial overlap between ground truth and segmented lesion in percentage is DSC and it is formulated using true positive (TPVF), false negative (FNVF), and false positive (FPVF) volume fractions. Specifically, if the ground truth and the segmented object are indicated by A_1 and A_2, then we have:

$$\mathrm{DSC}(A_1, A_2) = \frac{2 \times \mathrm{TPVF}}{(\mathrm{FPVF}+\mathrm{TPVF})+(\mathrm{TPVF}+\mathrm{FNVF})} \times 100. \tag{3}$$

Moreover, the Hausdorff distance (HD) [48] calculation was used to measure the maximum boundary deviation between two object boundaries. On considering the boundary of segmented objects as X and Y,

$$\mathrm{HD}(X, Y) = \max\left\{sup_{x \in X} inf_{y \in Y} d(x, y), sup_{y \in Y} inf_{x \in X} d(x, y)\right\}. \tag{4}$$

sup, *inf* indicate the supremum and infimum functions, whereas d denotes Euclidean distance.

Furthermore, errors in SUVmean uptake for the two methods, in reference to expert manual contouring, were

Copyright © 2016 Wolters Kluwer Health, Inc. All rights reserved.

Fig. 4

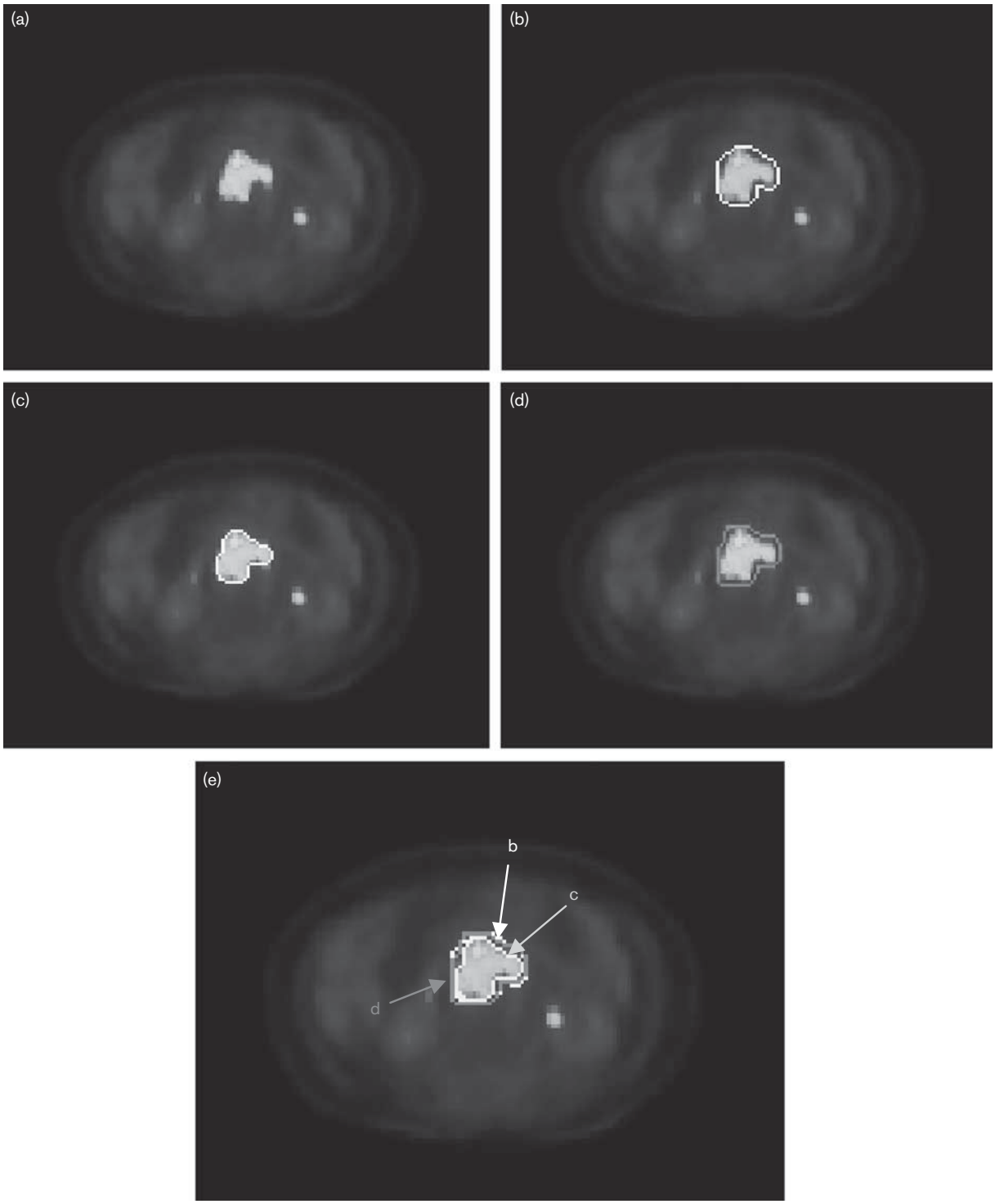

Application of different segmentation methods on a PET image of an abdominal tumor case: (a) original PET image, (b) expert manual contouring, (c) contours resulting from the random walker algorithm, and (d) contours resulting from the proposed fuzzy logic-based technique (d). The overlaid contours have been shown in (e).

Copyright © 2016 Wolters Kluwer Health, Inc. All rights reserved.

Fig. 5

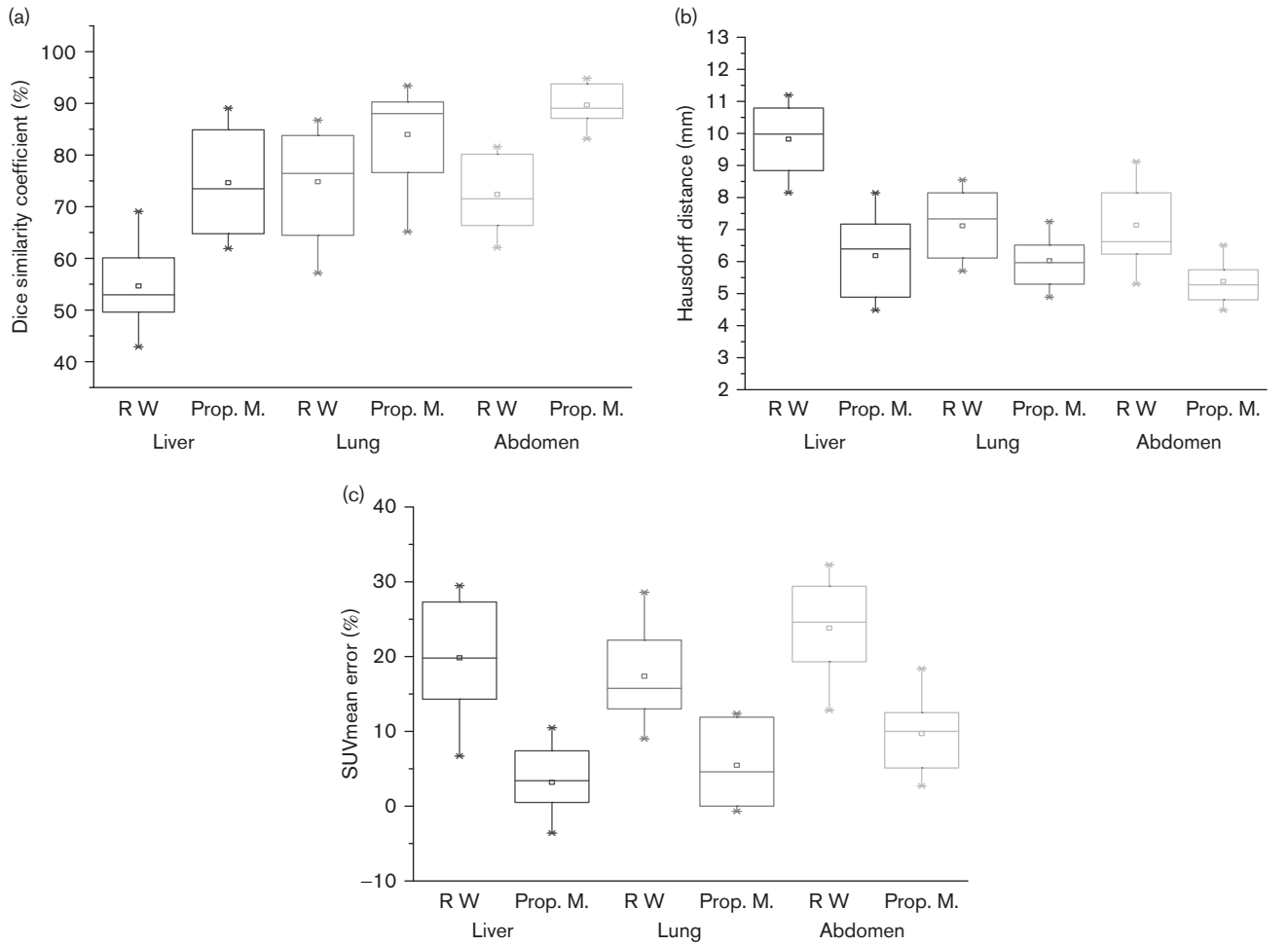

Plots of (a) DSC and (b) HD for tumor segmentation, as well as (c) SUVmean error, comparing the random walk (RW) with the proposed (Prop. M.) methods in relation to expert manual contouring in liver, lung, and abdominal tumors. DSC, dice similarity coefficient; HD, Hausdorff distance.

evaluated. All three abovementioned metrics were compared between the two methods using the paired *t*-test for assessment of statistical significance.

Results

In this section, the efficacy of the proposed technique in delineating uptake regions in clinical PET images is reported. The results of expert manual contouring, as well as random walker and proposed methods, are shown in Fig. 4a–e for qualitative analysis. A PET scan of an abdominal tumor has been illustrated in Fig. 4a, and manual expert contouring is shown in Fig. 4b. The results from the random walker and proposed segmentation methods, as well as an overall overlay, are shown in Fig. 4c–e, respectively.

Segmentation for liver, lung, and abdominal tumor PET images was performed including both RW and proposed techniques. Fig. 5a and b depicts the DSC and HD values, respectively, comparing the random walker and proposed fuzzy logic-based methods in the cases of liver, lung, and abdominal tumors. Mean DSC improvements (increase) from the random walker algorithm to the proposed method were 21.0 ± 7.2, 12.3 ± 5.8, and $18.4 \pm 6.1\%$ for liver, lung, and abdominal tumors, respectively (all statistically significant improvements with P-values < 0.001). For the HD metrics, the mean improvements (decrease) between the two methods were 3.6 ± 1.4, 1.3 ± 0.4, 1.8 ± 0.8 mm (all P-values < 0.001).

We subsequently investigated the effectiveness of the algorithm in tumor SUVmean value estimation. We thus assessed the performance of the RW versus proposed methods in estimation of SUVmean as compared with expert manual tumor delineation-based SUVmean. The average SUVmean errors obtained for the two methods are shown in Fig. 5c. The SUVmean errors were seen to reduce by 15.5 ± 6.3, 11.7 ± 8.6, and $14.1 \pm 6.8\%$ for liver, lung, and abdominal tumors, respectively (all P-values < 0.001).

Copyright © 2016 Wolters Kluwer Health, Inc. All rights reserved.

Fig. 6

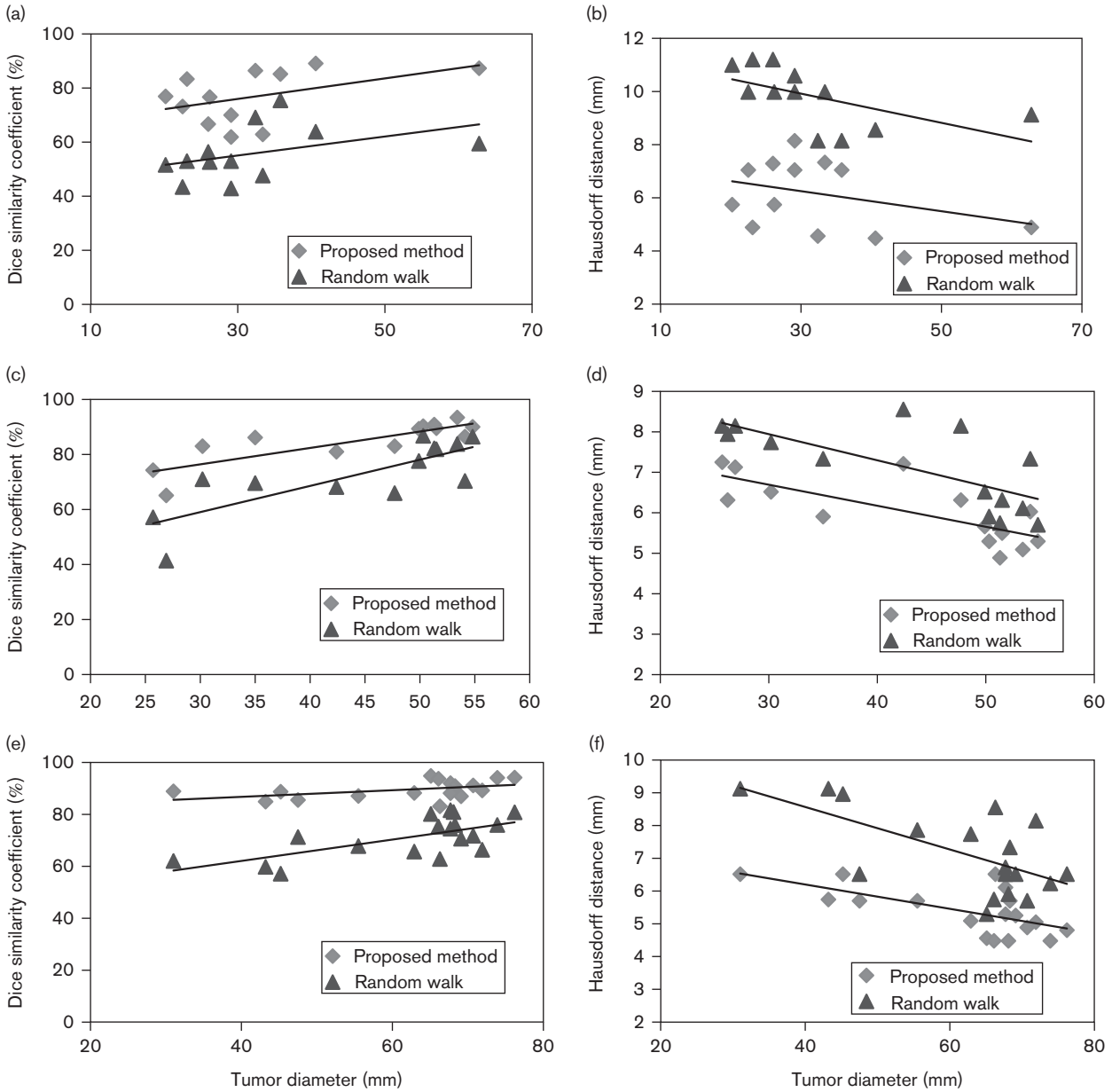

DSC (left) and HD (right) values as a function of the in-plane maximum diameter of tumor diameter for the random walker versus proposed methods in (a, b) liver, (c, d) lung, and (e, f) abdominal tumors. DSC, dice similarity coefficient; HD, Hausdorff distance.

To evaluate the performance of the proposed algorithm for different tumor diameters, the DSC and HD differences were investigated for a range of diameters. Figure 6 shows the DSC and HD differences between the random walker and proposed methods based on in-plane maximum diameters for different considered tumor sites. With increasing tumor diameter, DSC differences between the two methods show slight decreasing trends for lung and abdominal tumors. The proposed method thus illustrates overall improvements in DSC values in segmentation of smaller lung and abdominal tumors.

Furthermore, the impact of the activity concentration drop-off on the performance of the proposed algorithm was investigated using intensity line profile analysis along tumor edges. The ImageJ DICOM Viewer software (National Institutes of Health, Bethesda, Maryland, USA) was used to enable profile analysis. Two line profiles were considered, one along the maximum tumor diameter and the other perpendicular to it. Subsequently, the highest intensity gradient along each edge was considered as the edge-intensity slope. The mean of the slopes was reported as the edge-intensity gradient.

Copyright © 2016 Wolters Kluwer Health, Inc. All rights reserved.

Fig. 7

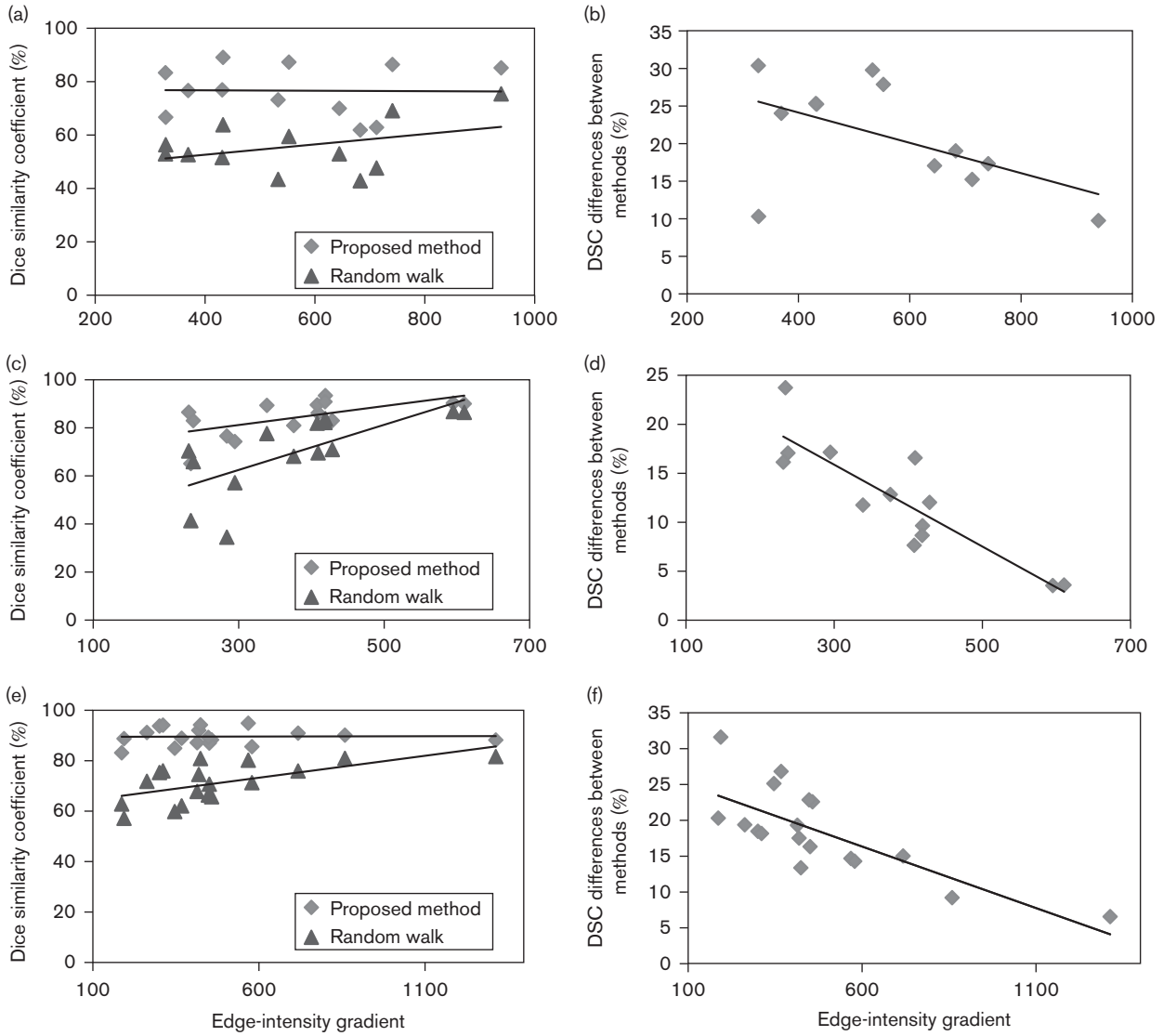

DSC values (left) and differences (right) as a function of tumor edge-intensity gradients for the random walker versus proposed methods in (a, b) liver, (c, d) lung, and (e, f) abdominal tumors. DSC, dice similarity coefficient.

The DSC and HD differences in terms of the edge-intensity gradient have been illustrated in Figs 7 and 8 for liver, lung, and abdominal tumor cases, respectively.

DSC and HD differences between two algorithms show that with increasing activity concentration drop-off at the edges of the tumors, the results from the two methods are close to each other, indicating that the proposed method becomes increasingly more effective in comparison with the random walker technique for low edge-intensity gradient cases.

Discussion

Functional volume segmentation techniques in PET imaging have garnered increasingly more attention in clinical applications [28]. Because of the limitations of PET imaging, specifically the presence of noise and PVE [15–18], tumor segmentation is especially challenged, and manual tumor delineation is subject to interobserver and intraobserver variability [49,50]. Thresholding approaches that have been widely used in clinical routine require additional anatomical information and parameter optimization using phantom studies.

The random walker algorithm, originally proposed by Grady [29], owing to its capabilities, has achieved increasing attention in tumor delineations of PET images. It is based on probability calculation of a pixel belonging to a tumor or background, and subsequently,

Copyright © 2016 Wolters Kluwer Health, Inc. All rights reserved.

Fig. 8

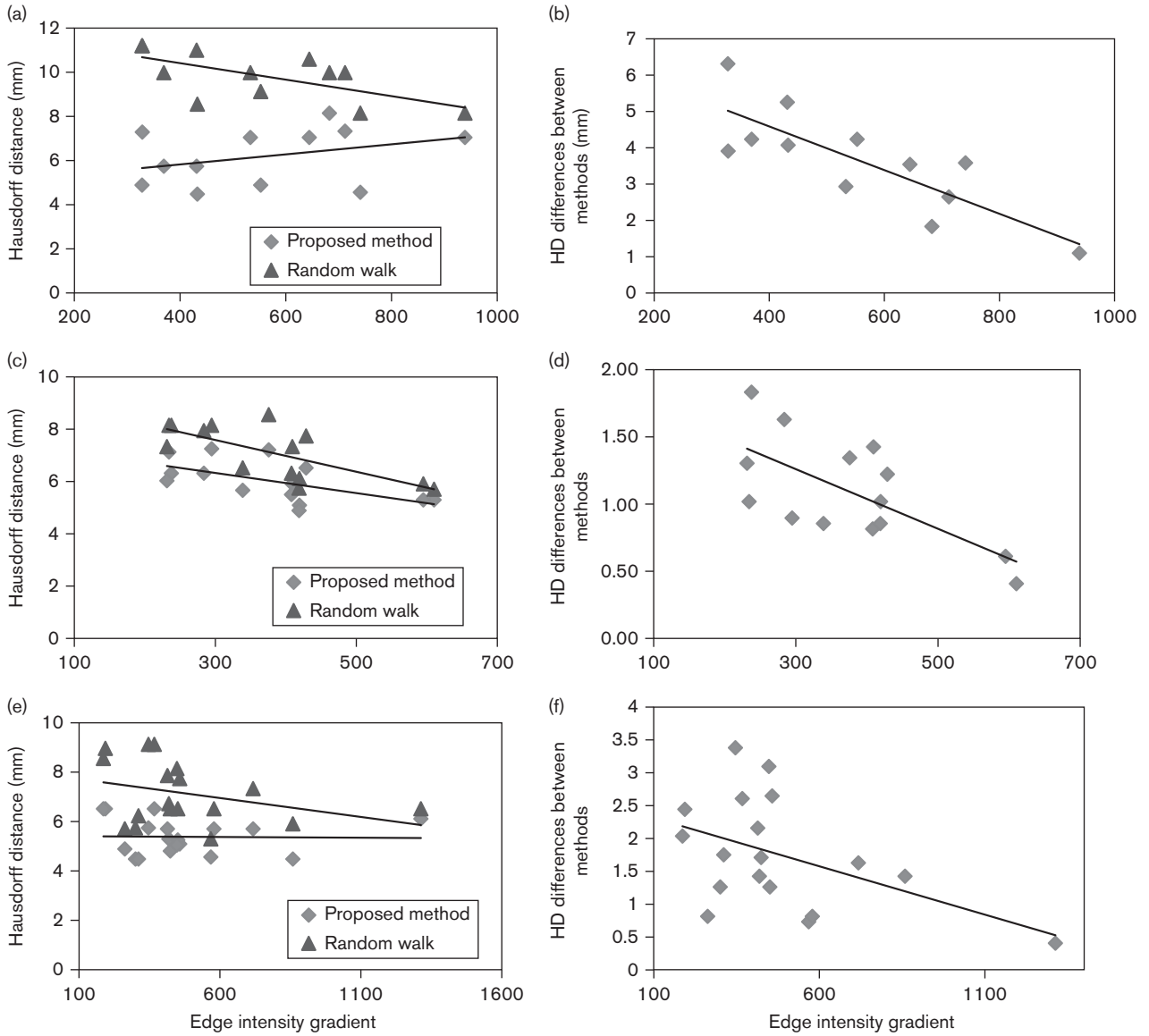

HD values (left) and differences (right) as a function of tumor edge-intensity gradients for the random walker versus proposed methods in (a, b) liver, (c, d) lung, and (e, f) abdominal tumors. HD, Hausdorff distance.

the pixel is labeled with the seeded label that achieves the highest probability.

In the present work, it was shown that hard decision-making in the pixel labeling process could reduce the efficiency of RW in PET tumor delineation. We selected tumor cases that were challenging with the RW algorithm, as they have low mean DSC and HD values in comparison with results reported in previous work [31, 34]. The mean DSC values for the random walker algorithm in our selected cases were 55.7 ± 9.9, 72.5 ± 13.0, and $71.2 \pm 7.7\%$ for liver, lung, and abdominal tumors, respectively. The mean HD values were 9.8 ± 1.1, 7.1 ± 1.0, and 7.1 ± 1.3 mm.

A fuzzy inference system was applied to detect tumor edges from the calculated probabilities in order to increase the edge-detection capability of the random walker algorithm. Thirty rules were utilized to consider all edge pixels in the image. The algorithm execution time was acceptable: the mean run time was ~ 2–3 s/tumor. Figure 5 illustrates the improved segmentation results using the proposed method in terms of DSC and HD, in comparison with random walk, in different

Copyright © 2016 Wolters Kluwer Health, Inc. All rights reserved.

clinical PET images. The mean DSC values for the proposed method were 76.7 ± 9.7, 84.8 ± 7.8, and 89.6 ± 3.4%, and the HD values were 6.2 ± 1.0, 5.7 ± 1 and 5.4 ± 0.7 mm for the three tumor sites, respectively.

Furthermore, errors in SUVmean estimation were investigated (Fig. 5c). Average errors for RW versus proposed methods were 19.8 ± 7.6 and 4.4 ± 2.6 for liver tumors, 17.4 ± 6.9 and 5.7 ± 3.1% for lung tumors, and 23.8 ± 6.8 and 9.7 ± 4.6% for abdominal tumors. The results showed significant improvements in tumor SUVmean estimations in clinical approaches (*P*-values mentioned in previous section).

To better assess the DSC and HD differences, as to when adding FIS to RW is most expected to improve the RW results, we looked for a parameter that described the differences in DSC and HD performance. The tumor-to-background contrast effect could be thought of, *a priori*, as a good descriptor. However, as the region of interest was drawn far away from the tumor edge in tumor and background regions for tumor-to-background contrast estimation, this parameter captured neither the DSC and HD difference behavior nor the edge-detection capability of the proposed method in comparison with the random walker algorithm.

The FIS is designed in such a way that it improves the edge-detection capability in RW. Therefore, a reliable technique could be tumor edge-intensity drop-off analysis. The results of DSC and HD differences as a function of edge-intensity gradient (Figs 7 and 8) show overall drop-off in the activity concentration: that is, the smaller the tumor edge, the greater the difference between the RW and propose algorithms. These results show a greater efficiency of the proposed technique in more blurred tumor edges and satisfy the goal of our study.

Moreover, tumor diameter analysis was implemented to evaluate the performance of the algorithm over a range of clinical tumor sizes. Results (Fig. 6) depict enhanced estimation of tumor edges at all tumor sites and special effectiveness of the proposed method in small lung and abdominal tumors.

Therefore, the proposed method could result in more accurate segmentation of blurred edges and small tumors in comparison with RW, which it makes the technique a powerful approach to PET image segmentation, in contrast to most previously proposed methods that fail to segment these challenging cases (small and low-contrast edges in tumors). It is worth mentioning that this technique could be easily extended to three dimensions, and it is fast enough for clinical application. As treatment target volume determination from functional imaging is increasingly being applied in radiation treatment planning approaches, and given the observed characteristics and results of the proposed approach, the technique may have the potential to enhance dose delivery in the target treatment volume, and we plan to evaluate its application in our future study.

Conclusion

In this study, a novel fuzzy logic-based framework to the random walker image segmentation algorithm was proposed and investigated. The performance of the method was evaluated for segmentation of clinical PET images including those of liver, lung, and abdominal tumors. The algorithm was shown to enable significant accuracy improvements in clinical PET data. Accuracy of the tumor segmentation and its execution time are favorable, and they make it a feasible and effective method for clinical applications. In future work, we plan to extend this work to three-dimensional segmentation algorithms and to evaluate their performance in PET tumor delineation as applied to radiation treatment planning applications.

Acknowledgements

Conflicts of interest

There are no conflicts of interest.

References

1 Wahl RL. *Principles and practice of PET and PET/CT*. Philadelphia, PA: Lippincott Williams & Wilkins; 2008.
2 Jarritt PH, Carson KJ, Hounsel AR, Visvikis D. The role of PET/CT scanning in radiotherapy planning. *Br J Radiol* 2006; **79**:27–35.
3 Krak N, Boellaard R, Hoekstra O. Effects of ROI definition and reconstruction method on quantitative outcome and applicability in a response monitoring trial. *Eur J Nucl Med Mol Imaging* 2005; **32**:294–301.
4 Larson SM, Erdi Y, Akhurst T, Mazumdar M, Macapinlac HA, Finn RD, *et al.* Tumor treatment response based on visual and quantitative changes in global tumor glycolysis using PET-FDG imaging. The visual response score and the change in total lesion glycolysis. *Clin Positron Imaging* 1999; **2**:159–171.
5 Pak K, Cheon GJ, Nam HY, Kim SJ, Kang KW, Chung JK, *et al.* Prognostic value of metabolic tumor volume and total lesion glycolysis in head and neck cancer: a systematic review and meta-analysis. *J Nucl Med* 2014; **55**:884–890.
6 Koyasu S, Nakamoto Y, Kikuchi M, Suzuki K, Hayashida K, Itoh K, *et al.* Prognostic value of pretreatment ^{18}F-FDG PET/CT parameters including visual evaluation in patients with head and neck squamous cell carcinoma. *Am J Roentgenol* 2013; **202**:851–858.
7 Kikuchi M, Koyasu S, Shinohara S, Usami Y, Imai Y, Hino M, *et al.* Prognostic value of pretreatment F-fluorodeoxyglucose positron emission tomography/CT volume-based parameters in patients with oropharyngeal squamous cell carcinoma with known p16 and p53 status. *Head Neck* 2015; **37**:1524–1531.
8 Paidpally V, Chirindel A, Chung CH, Richmon J, Koch W, Quon H, *et al.* FDG volumetric parameters and survival outcomes after definitive chemoradiotherapy in patients with recurrent head and neck squamous cell carcinoma. *Am J Roentgenol* 2014; **203**:W139–W145.
9 Chang KP, Tsang NM, Liao CT, Hsu CL, Chung MJ, Lo CW, *et al.* Prognostic significance of ^{18}F-FDG PET parameters and plasma Epstein-Barr virus DNA load in patients with nasopharyngeal carcinoma. *J Nucl Med* 2012; **53**:21–28.
10 Ryu IS, Kim JS, Roh JL, Lee JH, Cho KJ, Choi SH, *et al.* Prognostic value of preoperative metabolic tumor volume and total lesion glycolysis measured by ^{18}F-FDG PET/CT in salivary gland carcinomas. *J Nucl Med* 2013; **54**:1032–1038.
11 Abd El-Hafez YG, Moustafa HM, Khalil HF, Liao CT, Yen TC. Total lesion glycolysis: a possible new prognostic parameter in oral cavity squamous cell carcinoma. *Oral Oncol* 2013; **49**:261–268.
12 Zhang H, Wroblewski K, Liao S, Kampalath R, Penney BC, Zhang Y, *et al.* Prognostic value of metabolic tumor burden from F-18-FDG PET in surgical patients with non-small-cell lung cancer. *Acad Radiol* 2013; **20**:32–40.

Copyright © 2016 Wolters Kluwer Health, Inc. All rights reserved.

13 Liao SR, Penney BC, Zhang H, Suzuki K, Pu YL. Prognostic value of the quantitative metabolic volumetric measurement on ^{18}F-FDG PET/CT in stage IV nonsurgical small-cell lung cancer. *Acad Radiol* 2012; **19**:69–77.
14 Chen HHW, Chiu NT, Su WC, Guo HR, Lee BF. Prognostic value of whole-body total lesion glycolysis at pretreatment FDG PET/CT in non-small cell lung cancer. *Radiology* 2012; **264**:559–566.
15 Rousset OG, Rahmim A, Alavi A, Zaidi H. Partial volume correction strategies in PET. *PET Clinics* 2007; **2**:235-249.
16 Soret M, Bacharach SL, Buvat I. Partial-volume effect in PET tumor imaging. *J Nucl Med* 2007; **48**:932–945.
17 Erlandsson K, Buvat I, Pretorius PH, Thomas BA, Hutton BF. A review of partial volume correction techniques for emission tomography and their applications in neurology, cardiology and oncology. *Phys Med Biol* 2012; **57**: R119–R159.
18 Rahmim A, Qi J, Sossi V. Resolution modeling in PET imaging: theory, practice, benefits, and pitfalls. *Med Phys* 2013; **40**:064301.
19 Hatt M, Cheze Le Rest C, Descourt P, Dekker A, De Ruysscher D, Oellers M, *et al*. Accurate automatic delineation of heterogeneous functional volumes in positron emission tomography for oncology applications. *Int J Radiat Oncol Biol Phys* 2010; **77**:301–308.
20 Nestle U, Kremp S, Schaefer-Schuler A, Sebastian-Welsch C, Hellwig D, Rübe C. Comparison of different methods for delineation of ^{18}F-FDG PET-positive tissue for target volume definition in radiotherapy of patients with non-small cell lung cancer. *J Nucl Med* 2005; **46**:1342–1348.
21 Drever L, Robinson D, McEwan A, Roa W. A local contrast based approach to threshold segmentation for PET target volume delineation. *Med Phys* 2006; **33**:1583–1594.
22 van Baardwijk A, Bosmans G, Boersma L, Buijsen J, Wanders S, Hochstenbag M. PET-CT-based auto-contouring in nonsmall- cell lung cancer correlates with pathology and reduces interobserver variability in the delineation of the primary tumor and involved nodal volumes. *Int J Radiat Oncol Biol Phys* 2007; **68**:771–778.
23 Jentzen W, Freudenberg L, Eising E, Heinze M, Brandau W, Bockisch A. Segmentation of PET volumes by iterative image thresholding. *J Nucl Med* 2007; **48**:108–114.
24 Vees H, Senthamizhchelvan S, Miralbell R, Weber D, Ratib O, Zaidi H. Assessment of various strategies for ^{18}F-FET PET guided delineation of target volumes in high-grade glioma patients. *Eur J Nucl Med Mol Imaging* 2009; **36**:182–193.
25 Davis JB, Reiner B, Huser M. Assessment of ^{18}(F) PET signals for automatic target volume definition in radiotherapy treatment planning. *Radiother Oncol* 2006; **80**:43–50.
26 Foster B, Bagci U, Mansoor A, Xu Z, Mollura D. A review on segmentation of positron emission tomography images. *Comput Biol Med* 2014; **50**:76–96.
27 Zaidi H, Abdoli M, Fuentes CL, El Naqa IM. Comparative methods for PET image segmentation in pharyngolaryngeal squamous cell carcinoma. *Eur J Nucl Med Mol Imaging* 2012; **39**:881–891.
28 Zaidi H, El Naqa I. PET-guided delineation of radiation therapy treatment volumes: a survey of image segmentation techniques. *Eur J Nucl Med Mol Imaging* 2010; **37**:2165–2187.
29 Grady L. Random walks for image segmentation. *IEEE Trans Pattern Anal Mach Intell* 2006; **28**:1–17.
30 Onoma DP, Ruan S, Gardin I, Monnehan GA, Modzelewski R, Vera P. 3D random walk based segmentation for lung tumor delineation in PET imaging. Biomedical Imaging (ISBI) 2012 9th IEEE International Symposium; 2-5 May 2012, Barcelona, Spain. pp. 1260–1263.
31 Soufi M, Kamali Asl AR, Geramifar P. Random walk algorithm seed localization parameters in lung positron emission tomography (PET) images. *Med Phys* 2015; **42**:3221.
32 Fechter T, Mix M, Gardin I, Papke T, Schimek-Jasch T, Meyer P, *et al*. Malignant glioma delineation in amino acid PET-images using a 3D random walk approach. *Int J Radiat Oncol Biol Phys* 2013; **87**:S622.
33 Hui C, Xiuying W, Fulham M, Feng DD. Prior knowledge enhanced random walk for lung tumor segmentation from low-contrast CT images. *Conf Proc IEEE Eng Med Biol Soc* 2013; **2013**:6071–6074.
34 Bagci U, Udupa JK, Mendhiratta N, Foster B, Xu Z, Yao J, *et al*. Joint segmentation of anatomical and functional images: Applications in quantification of lesions from PET, PET-CT, MRI-PET, and MRI-PET-CT images. *Med Image Anal* 2013; **17**:929–945.
35 Bagci U, Udupa J, Yao J, Mollura D. Co-segmentation of functional and anatomical images. *Med Image Comput Comput Assist Interv* 2012; **7512**:459–467.
36 Bagci U, Yao J, Caban J, Turkbey E, Aras O, Mollura D. A graph-theoretic approach for segmentation of pet images. *Conf Proc IEEE Eng Med Biol Soc* 2011; **2011**:8479–8482.
37 Ganesh M. *Introduction to fuzzy sets and fuzzy logic*. New Delhi: Prentice-Hall; 2008. pp. 169–233.
38 Alshennawy AA, Aly AA. Edge detection in digital images using fuzzy logic technique. *World Acad Sci Eng Technol* 2009; **51**:178–186.
39 Kaur EK, Mutenja EV. Fuzzy logic based image edge detection algorithm in MATLAB. *IJCA* 2010; **1**:55–58.
40 Begol M, Maghooli K. Improving digital image edge detection by fuzzy systems. *World Acad Sci Eng Technol* 2011; **81**:76–79.
41 Barkhoda W, Akhlaqian Tab F, Shahryari OK. Fuzzy edge detection based on pixel's gradient and standard deviation values. Computer Science and Information Technology, 2009 IMCSIT'09 International Multiconference; 12-14 October 2009, Mragowo, Poland. pp. 7–10.
42 Dinesh Kumar J, Mohan V. Edge detection in the medical MR brain image based on fuzzy logic technique. International Conference of Information Communication and Embedded Systems (ICICES), 27-28 February 2014, Chennai, India. pp. 1–9.
43 Bloch I. Fuzzy methods in medical imaging. In: Paragios N, Duncan J, Ayache N, editors. *Handbook of biomedical imaging*. US: Springer; 2015. pp. 25–44.
44 Rashmi KA, Kusagur DA. An improved fast edge detection for medical image based on fuzzy techniques. *Fuzzy Sys* 2012; **4**:147–150.
45 Chaira T, Ray AK. Construction of fuzzy edge image using interval type II fuzzy set. *Int J Comput Int Sys* 2013; **7**:686–695.
46 Yen J, Langari R. *Fuzzy logic: intelligence, control, and information*. Upper Saddle River, NJ: Prentice-Hall; 1999. pp. 120–603.
47 Dice L. Measures of the amount of ecologic association between species. *Ecology* 1945; **26**:297–302.
48 Cignoni P, Rocchini C, Scopigno R. Metro: measuring error on simplified surfaces. *Computer Graphics Forum* 1998; **18**:167–174.
49 Paidpally V, Mercier G, Shah BA, Senthamizhchelvan S, Subramaniam RM. Interreader agreement and variability of FDG PET volumetric parameters in human solid tumors. *Am J Roentgenol* 2014; **202**:406–412.
50 Shah B, Srivastava N, Hirsch AE, Mercier G, Subramaniam RM. Intra-reader reliability of FDG PET volumetric tumor parameters: effects of primary tumor size and segmentation methods. *Ann Nucl Med* 2012; **26**:707–714.

Copyright © 2016 Wolters Kluwer Health, Inc. All rights reserved.